CrossMark

Comparative Study of Iron-Based Fischer–Tropsch Synthesis Catalysts Promoted with Strontium or Potassium
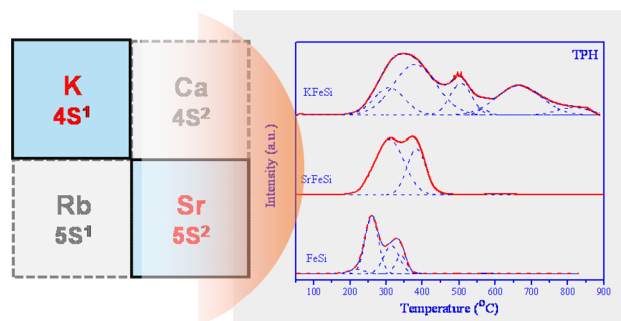
Jifan Li[1] · Xiaofan Cheng[2] · Chenghua Zhang[1] · Wensheng Dong[3] · Yong Yang[1] ·
Yongwang Li[1]

Abstract The effect of strontium as a chemical promoter on iron-based Fischer–Tropsch synthesis (FTS) catalysts was investigated and compared with that of potassium. Strontium was chosen for study because of its relationship to potassium through the Diagonal relationship in the Periodic Table. The catalysts were characterized by N_2 physisorption, X-ray diffraction, laser Raman spectroscopy, Mössbauer effect spectroscopy, H_2/CO temperature programmed reduction and temperature programmed hydrogenation. FTS reaction was tested in a fixed-bed reactor. It was found that strontium and potassium strengthened Fe-O bonds of iron oxides species, which is not favorable for the reduction of the catalysts in H_2. Both of them enhanced the reduction and carbonization of the catalysts in CO and syngas atmosphere, suppressed the hydrogenation of surface carbon species, however, strontium is less effective than potassium. Besides, strontium improved the dispersion of iron oxide. Strontium did not significantly affect the activity of FTS and water gas shift (WGS), but facilitated the oxidation of iron carbides to Fe_3O_4 during FTS reaction process, while potassium significantly improved the FTS and WGS activity and inhibited the oxidation of iron carbide. Both of strontium and potassium decreased the selectivity of methane while facilitated the formation of heavy hydrocarbons and olefin, whatever, strontium exhibited a weaker effect compared to potassium.

Graphical Abstract

1 Introduction

Fischer–Tropsch synthesis (FTS) is a well-established industrial route to convert syngas made from coal, natural gas or biomass into hydrocarbons [1]. Considering the limited supply and non-renewable nature of crude oil, FTS attracts increasing attention as an alternative way to produce petrochemical substitutes and fuels [2]. Iron-based catalysts are favorably applied in FTS processes for their low price,

✉ Jifan Li
tjuljf@aliyun.com

✉ Chenghua Zhang
zhangchh@sxicc.ac.cn

1 State Key Laboratory of Coal Conversion, Institute of Coal Chemistry, Chinese Academy of Sciences, Taiyuan 030001, People's Republic of China

2 Shaanxi Coal and Chemical Industry Technology Development Centre Co., LTD, Xi'an 710062, People's Republic of China

3 Key Laboratory of Applied Surface and Colloid Chemistry (SNNU), MOE, School of Chemistry and Chemical Engineering, Shaanxi Normal University, Xi'an 710062, People's Republic of China

high FTS and water-gas shift (WGS) activities, and broad operation conditions [3]. However, chemical promoters (K, Cu, Mn, Zr, Mo, and others) are usually introduced into iron-based catalysts to facilitate the reduction or improve the catalysts activity and selectivity [4].

Potassium is normally added to iron-based catalysts as a chemical promoter [5]. The influence of potassium on the performances of iron-based catalyst has been studied extensively [5–12]. Potassium is reported to facilitate the chain propagation reaction, olefins formation [5, 8], the carburization of catalysts [13], but suppress the formation of CH_4 [12]. The effect of potassium on the catalyst activity is dependent on its contents added [12]. The modification of potassium also has positive influence on the WGS activity [5, 8]. Additionally, numerous studies also have been performed to evaluate the promotional effects of Group I alkali metals on FTS performances of iron-based catalysts [14–16]. Dry et al. [14] found that the surface basicity of alkalis promoted catalysts, measured by the adsorption of CO_2, inclined following the sequence of $Ba < Li < Ca < Na < K$. The higher surface basicity led to lower methane selectivity in FTS. However, Ngantsoue-Hoc and Davis [16] observed that the relative impact of Group I alkali metals depended upon the conversion level, but potassium promoted catalysts had the highest activity at all conversion levels.

The chemical properties of alkaline earth metals are similar to alkali metals, at the same time, their oxides have some properties similar to supporter (such as silica and alumina) [17, 18]. Therefore, alkaline earth metals are considered as useful additives for iron-based FTS catalysts. Mg or Ca was reported to low the methane selectivities, and improve stability of iron-based FTS catalysts [19–22]. Luo et al. [23] investigated the promotion of alkaline earth metals without strontium on iron-based FTS catalysts using a continuous stirred tank reactor (CSTR). They concluded that the addition of alkaline earth metals decreased the gas product rate but improved the total liquid fraction product rate. Li et al. [24] compared the promotional effects of alkaline earth metals on iron-based FTS catalysts using a fixed bed reactor. They found that alkaline earth metals decreased the selectivities to methane but enhanced the formation of the heavy weight hydrocarbons and olefin, moreover, strontium was the most effective promoter among alkaline earth metals.

In spite of the recognized importance of the alkali and alkaline earth metals promoters, studies to compare their relative promotional effects are hardly reported. Except for elements in a group in the Periodic Table, elements with Diagonal relationships would also have similar properties, which is useful to exploit promoters of catalysts. With this in mind we decided to investigate the promotional effects of strontium on iron-based catalysts for FTS and compare to that of potassium, because of their relationship in the Periodic Table to each other through the Diagonal relationship. Furthermore,

little work has been performed to study the influences of strontium on iron-based FTS catalysts. No research has been carried out to compare the influence of strontium to potassium on iron-based catalysts for FTS, to the best of our knowledge.

The objective of the present study is to compare the promotion effects of strontium and potassium on precipitated Fe/SiO_2 catalysts. A combination of precipitation and spray-drying method was employed to prepared the catalysts. Several techniques, including N_2 physisorption, Raman spectroscopy (LRS), Mössbauer spectroscopy (MES), H_2/CO temperature-programmed reduction (TPR), X-ray diffraction (XRD), and temperature-programmed hydrogenation (TPH), were used to characterize the catalysts. The catalysts were evaluated in a fixed-bed reactor. Their FTS performance was correlated with the results of characterization.

2 Experimental

2.1 Catalyst Preparation

A combination of co-precipitation and spray-dried method was employed to prepare the catalysts used in this study. In brief, a solution including silica sol and $Fe(NO_3)_3$ with an atomic ratio of Si/Fe = 5:100 was precipitated at pH = 8.5–9.0 and T = 70 °C using NH_4OH solution. The obtained precipitate was completely washed with deionized water, and followed by filtering. After that, the potassium and strontium were introduced by wetness impregnation using an aqueous potassium or strontium nitrate to obtain an atomic ratio of A (A: potassium or strontium)/Fe = 2/100. The mixture was re-slurried and spray-dried. The spray-dried powder was calcined at 500 °C for 5 h. The samples were designed FeSi, SrFeSi, and KFeSi.

2.2 Catalyst Characterizations

The concentration of the metal in the catalyst was determined by an Induced Coupled Plasma-Optical Emission Spectrometry (ICP-OES, Thermo Icap 6300, USA).

The morphologies of the catalyst samples and the elemental concentrations of the catalyst surfaces and elemental distributions were studied using scanning electron microscopy (SEM) and energy dispersive X-ray spectroscopy (EDS). SEM and EDS were performed using a scanning electron microscope (SEM, FEI Quanta 400 F) and an energy dispersive X-ray spectrometer (EDS). Before the EDS test, the grinded catalyst was pressed into a tablet.

The textural properties of the fresh catalysts were determined via N_2 physisorption at −196 °C, using a Micromeritics ASAP 2420 instrument. Before to the measurement, the catalysts were degassed under vacuum at 90 °C for 1 h and 350 °C for 8 h.

Laser Raman spectroscopy was measured on LabRAM HR800 (HORIBA JOBINYVON) equipping an air cooled frequency doubled Nd: Yag laser ($\lambda = 532$ nm) as the ray source and CCD as the detector.

Powder X-ray diffraction patterns were measured on a Bruker D8 Advance X-ray diffractometer with Cu Kα radiation ($\gamma = 1.5406$ Å). A step scan mode was used with a scan rate of $0.02°$ (2θ) per second from $20°$ to $80°$.

The Mössbauer spectra of samples were acquired on MR-351 constant-acceleration Mössbauer spectrometer (FAST, Germany) at room temperature. The radioactive source was 25-mCi[57]Co in a Pd matrix. The spectrometer was operated in a symmetric constant acceleration mode. The spectra were collected over 512 channels in the mirror image format.

H_2/CO-TPR were carried out using a dynamic analyzer (Micromeritics, Model 2920). About 40 mg of sample was loaded in a U-type quartz tube reactor. The reactor was heated from room temperature to $900 °C$ at a heating rate of $10 °C/min$. The samples were treated with 50 ml/min reducing gas composed of 10% H_2/90% Ar (H_2-TPR) or in 5% CO 95% He (CO-TPR).

Temperature-programmed hydrogenation (TPH) was carried out in the same instrument as TPR. About 100 mg of catalyst was loaded into the quartz tube reactor. The catalyst was firstly pretreated with 5% CO/95% He at $300 °C$ for 10 h, and then cooled to $50 °C$. Following, the pretreated catalyst was swept by pure H_2 until the signal leveled off. After that, the reactor was heated from room temperature to $800 °C$ at a heating rate of $10 °C/min$. The CH_4 (TPH, m/z$=15$) signals were detected with on-line quadruple mass spectrometer.

2.3 FTS Performance

The FTS experiments were carried out in a 12 mm i.d. stainless steel tubular reactor. For all the experiments, 3 g catalyst was filled into the isothermal region of reactor, and the residual volume of the reactor was filled with quartz granules with diameter of 40–60 mesh. All the tested samples were reduced in situ with a stream of syngas (H_2/CO$=2.0$) under $280 °C$, 1 atm, and $1000 \, h^{-1}$ for 20 h. The FTS reaction was carried out in a flow of syngs at $260 °C$, 1.5 MPa, and $2000 \, h^{-1}$. The product analysis system has been detailedly described elsewhere [25].

3 Results and Discussion

3.1 BET, SEM-EDS and Raman Characterizations of the Fresh Catalysts

Table 1 lists the results of N_2 physisorption for the fresh catalysts. The addition of potassium does not remarkably

alter the surface area and the average pore diameter of the fresh catalyst. In contrast, the modification of strontium increases the surface area and decreases the average pore diameter of the catalyst by about 20%. This indicates that the addition of strontium improves the dispersion of iron oxide.

Catalyst granule morphologies for all the calcined catalysts observed using SEM is displayed in Fig. 1. In general, the catalyst granules show spherical structure. No apparent difference in granule morphologies among the unprompted and promoted catalysts is observed. EDS mapping was used to analyze the elemental distribution on the surface of the calcined catalyst particles. As seen in Fig. 1, all elements are well distributed on the surface of the catalyst particles, with no obvious segregation.

The Raman spectra of fresh catalysts are presented in Fig. 2. The spectrum of the unprompted catalyst contains typical peaks of the Fe–O bond for hematite (α-Fe_2O_3) situated at 217, 283 and 392 cm^{-1} [26]. For the promoted catalysts, two additional peaks are observed at 244 and 497 cm^{-1}, which is also assigned to the characteristic bands of α-Fe_2O_3. It indicates that α-Fe_2O_3 is the main species in the fresh catalysts. Furthermore, these Fe–O bands shift to higher frequency with the introduction of strontium and potassium. The happening of blue-shifts implies that Fe–O bond is strengthened by the incorporation of strontium and potassium.

3.2 Crystallite Structure of Catalysts

Figure 3a displays the XRD patterns for the fresh catalysts. The only visible phase identified in XRD patterns of the fresh catalysts is α-Fe_2O_3, which contains typical bands at 2θ values of $24.2°$, $33.1°$, $35.6°$, $40.8°$, $49.5°$, $54.0°$, $57.6°$, $62.5°$ and $64.0°$. The Mössbauer spectra of the fresh catalysts are presented in Fig. 3b, and the spectra parameters are tabulated in Table 2. The Mössbauer spectra of the FeSi and KFeSi catalysts include only a sextet, which corresponds to the magnetic α-Fe_2O_3 with large srystallites [12]. For the SrFeSi catalyst, in addition to a sextet, a doublet is also

Table 1 The composition and BET results of the fresh catalysts

Catalysts	Catalyst composition (atomic ratio)[a]	Surface area[b] (m²/g)	Pore volume (cm³/g)	Average pore size (nm)
FeSi	100Fe4.6Si	50	0.20	12.6
SrFeSi	1.9Sr100Fe4.5Si	62	0.19	10.0
KFeSi	2.1K100Fe4.6Si	53	0.19	11.8

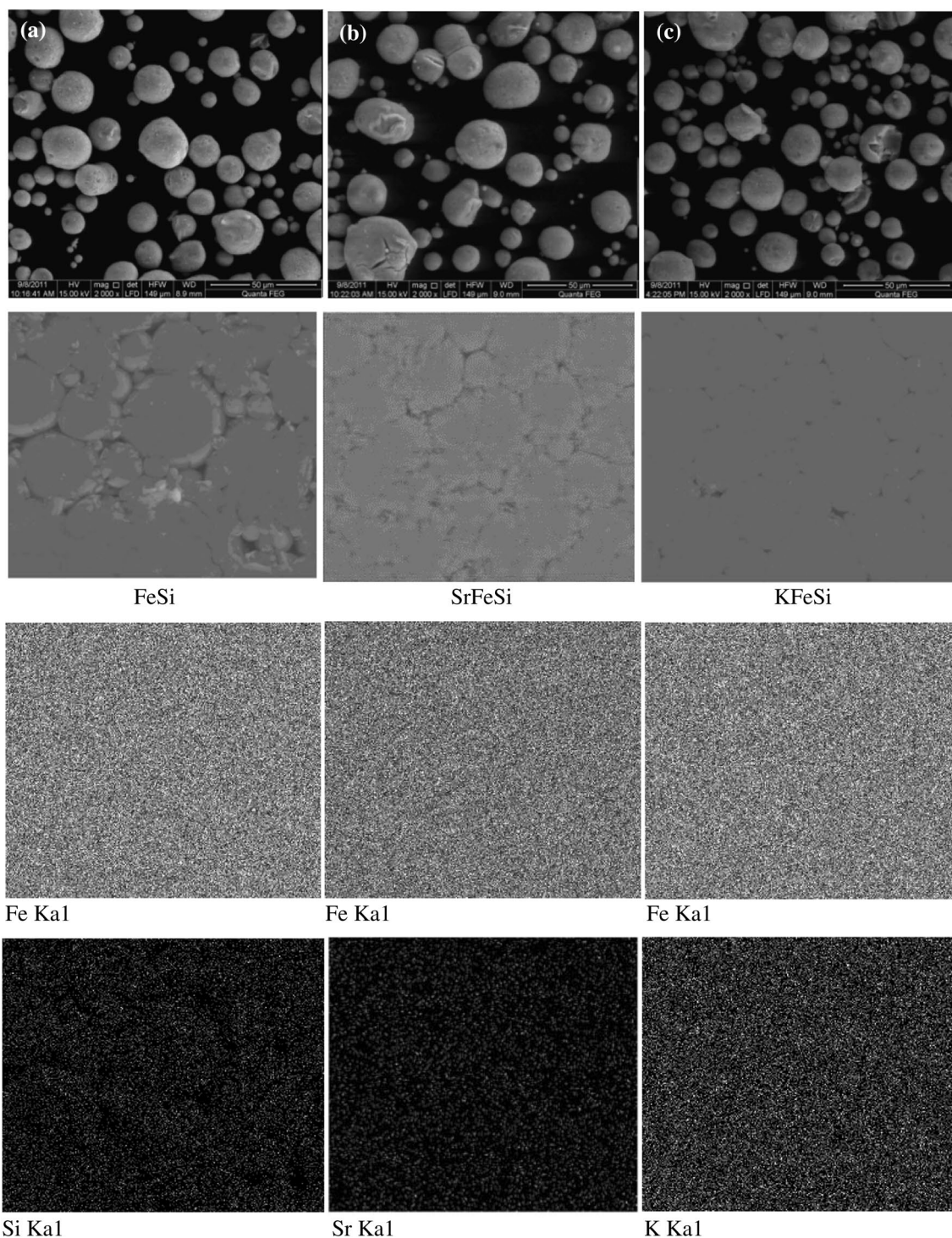[a]ICP-OES results. Max error$=\pm5\%$

[b]Max error$=\pm5\%$

Fig. 1 SEM micrographs and EDS mapping of fresh catalysts: **a** FeSi; **b** SrFeSi; and **c** KFeSi

observed in the Mössbauer spectra, which is attributed to the superparamagnetic Fe^{3+} (spm Fe^{3+}) ions on the non-cubic sites with crystallite size smaller than 13.5 nm [27]. According to the spectral area (Table 2), the unprompted and potassium promoted catalysts are composed of 100% ferromagnetic α-Fe_2O_3. However, about 25.6% of spm Fe^{3+} is found in the SrFeSi catalyst. These results further confirm that the addition of potassium has no apparent influences on the dispersion of iron oxide species, whereas the dispersion of iron oxide is improved with the promotion of strontium. The results of MES consist with those of BET and XRD characterizations.
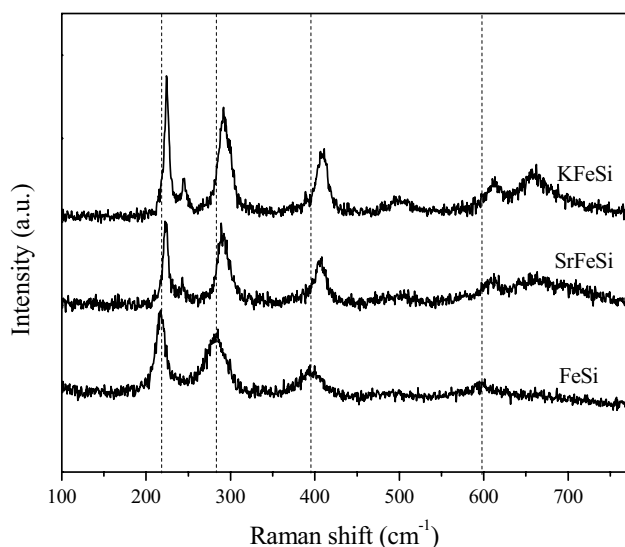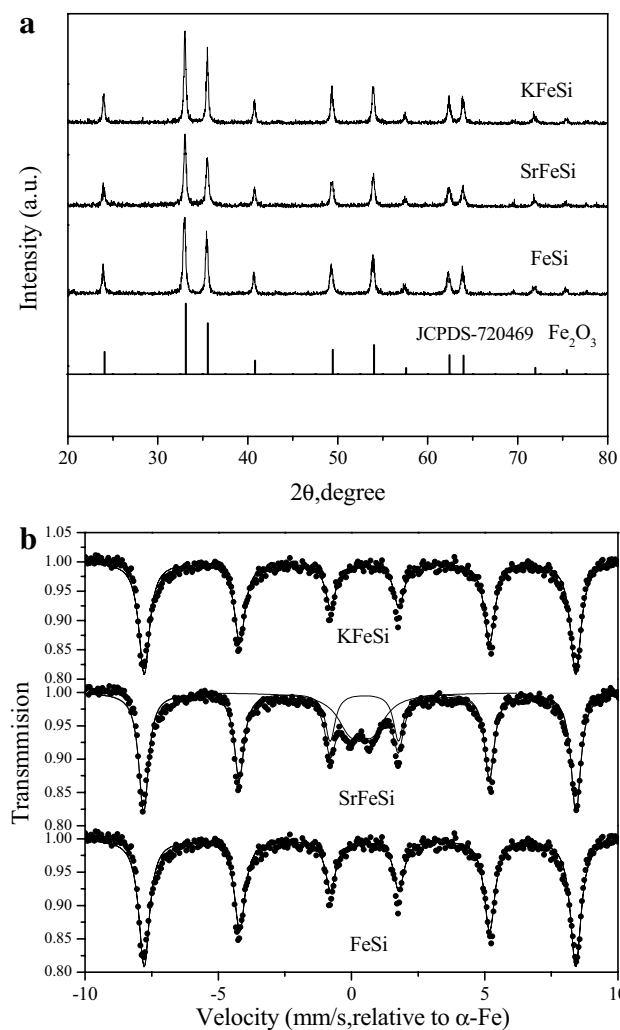
Fig. 2 Raman spectra of the fresh catalysts

Fig. 3 XRD patterns (**a**) and Mössbauer spectra (**b**) of the fresh catalysts

The activated catalysts were characterized with XRD and MES. The XRD patterns and Mössbauer spectra are displayed in Fig. 4a, b, respectively. The MES parameters are summarized in Table 3. In the XRD patterns, only the typical peaks of the magnetite located at 30.1°, 35.5°, 37.1°, 43.1°, 57.0°, and 62.6° can be observed, whereas the peak intensities decrease in order of FeSi, SrFeSi and KFeSi. There is no iron carbides can be observed, which is ascribed to the poor crystal shape of iron carbides or the amount of iron carbides in the activated catalysts beyond the XRD detectability. As shown in Fig. 4b, the MES spectra of the FeSi and KFeSi catalysts include several sets of sextets, whereas a doublet beside sextets is detected in the spectra of the strontium promoted catalyst. The sextets with Hhf of 485 ± 1 and 455 ± 2 kOe are ascribed to the tetrahedral and octahedral sites of Fe_3O_4 [28]. Other sextets with Hhf of 213–228, 175–183 and 110 kOe belong to the three different sites of stoichiometric χ-Fe_5C_2 [12]. The doublet is responded to superparamagnetic Fe^{2+} with size smaller than 13.5 nm [21]. After reduction, Fe_3O_4 is the main phase for all catalysts, which is consistent with XRD results. The content of iron carbide increases slightly for the SrFeSi catalyst, while is largely improved for the KFeSi catalyst compared to that for the FeSi catalyst. These results imply that the addition of strontium and potassium facilitates the carburization of catalysts, while the incorporation of strontium is less promotional than the addition of potassium.

The XRD patterns of catalysts after reaction are shown in Fig. 5a. Only the characteristic peaks of the magnetite can be observed in the XRD patterns of FeSi and SrFeSi catalysts. However, for the KFeSi catalyst, in addition to the characteristic peaks of the magnetite phase, the typical peaks of iron carbide (39.3°, 43.5°, 44.1° and 45.0°) are also observed. MES was employed to further measure the composition of the used catalysts. The Mössbauer spectra are displayed in Fig. 5b and the phase compositions are listed in Table 4. Compared with the activated samples, it can be found that the content of iron carbide decreases sharply while the amount of magnetite increases for the FeSi and SrFeSi catalysts. The spm Fe^{2+} also apparently decreases for SrFeSi catalyst. This is probably due to the re-oxidization of χ-Fe_5C_2 and spm Fe^{2+} to magnetite or spm Fe^{3+} during FTS reaction [29]. For KFeSi catalyst, the content of iron carbide increases remarkably after FTS reaction, which is ascribed to the further reduction and carburization during the FTS reaction [12].

3.3 Reduction and Carburization Behaviors

Figure 6a shows the H_2-TPR profiles of the catalysts. In the profiles of all catalysts, two well-separated H_2 consumption peaks can be detected, which is the features of the two-step reduction of iron-based catalysts from α-Fe_2O_3 to Fe_3O_4 and

Table 2 Mössbauer spectra parameters of the fresh catalysts

Catalysts	IS (mm/s)	QS (mm/s)	Hhf (kOe)	Area[a] (%)	Assignment
FeSi	0.41	−0.18	504	100.0	α-Fe_2O_3
SrFeSi	0.40	−0.17	504	74.4	α-Fe_2O_3
	0.37	0.81		25.6	Fe^{3+}
KFeSi	0.40	−0.17	505	100.0	α-Fe_2O_3

[a]Max error = ±1 %
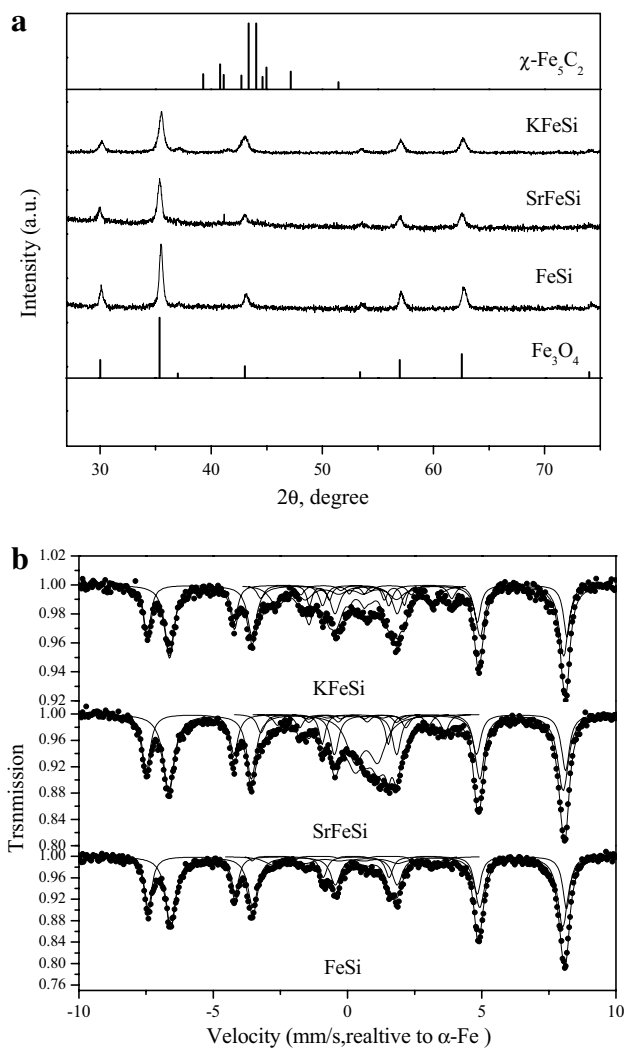
Fig. 4 XRD patterns (**a**) and Mössbauer spectra (**b**) of the reduced catalysts

Fe_3O_4 to α-Fe [30]. It is clear that the addition of potassium shifts the position of reduction peaks to higher temperatures. A similar but weaker effect is observed with the modification of strontium. These results clearly indicate that the addition of potassium and strontium severely inhibits the reduction of catalysts, while the incorporation of strontium shows a relative weak effect. This perhaps result from the interaction between promoters (potassium or strontium)

and iron oxide, which in turn enhances Fe–O bonds in iron oxides. The strengthened Fe–O bonds are difficult to cleave, leading to higher temperature in the H_2-TPR process.

The CO-TPR profiles of the catalysts are shown in Fig. 6b. A tiny peak ahead 280 °C exists on all the profiles of the catalysts. This perhaps result from somewhat easily reduced species. For FeSi catalyst, three apparent reduction/carburization peaks can be observed. The first peak located at 290–320 °C can be attributed to the reduction of Fe_2O_3 to Fe_3O_4. Apparently, the temperature of this reduction peak slightly increases with the addition of potassium and strontium. This step is a process for removal of lattice oxygen from the bulk iron oxide by the reaction with CO [25, 31]. As mention in the forgoing sections, the modification of potassium and strontium would strengthen Fe–O bonds in α-Fe_2O_3. The strengthened Fe–O bonds are difficult to cleave, which in turn is not favorable for the reduction of Fe_2O_3 to Fe_3O_4 and leads to an increase of the reduction temperature. The second peak at 400–650 °C is attributed to the carburization of catalyst, while the peak above 650 °C is ascribed to the carburization of the iron oxide species difficultly reduced. The promotion of strontium presents apparently influence on the carburization peaks. It enlarges the first carburization peak and weakens the peak behind 650 °C. The incorporation of potassium is more effective on the carburization peaks. That is, the first carburization peak is further enlarged and shifts to low temperature, even the peak behind 650 °C almost disappears. These results suggest that the addition of potassium and strontium facilitates the carburization of catalysts, whereas the addition of strontium shows a relative weak effect. This is ascribed to the different promotion of potassium and strontium on the CO dissociation adsorption of catalysts. Potassium significantly facilitates the CO dissociation adsorption of catalysts due to its strong basicity, which in turn improves the carburization of catalysts [32]. Strontium has weaker basicity than potassium. Hence, strontium would be less effective on enhancing the adsorption of CO, as a result, strontium shows a relative weak influence on the carburization of catalysts than potassium.

The reduction of the catalysts in syngas is presented in Fig. 7. The concentration of CO_2 in the tail gas during in situ pretreatment could qualitatively reflect the reduction degree of the catalysts [25]. As displayed in Fig. 7, when the pretreated temperature increases to 280 °C and remains constant, the CO_2 concentration of FeSi catalyst grows slowly from a low to a high level and declines slightly with the increase of time on stream. A similar variation tendency with slight higher CO_2 concentration is observed over SrFeSi catalyst. However, that of KFeSi catalyst increases quickly to a much higher level (ca. 10.1 %) and also decreases slightly thereafter with increasing reduction time. It is evident that the addition of potassium and strontium facilitates the reduction

Table 3 Mössbauer spectra parameters of the reduced catalysts

Catalysts	IS (mm/s)	QS (mm/s)	Hhf (kOe)	Area[a] (%)	Assignment
FeSi	0.35	0.04	484	31.0	Fe_3O_4 (A)
	0.71	0.02	454	56.0	Fe_3O_4 (B)
	0.16	−0.09	228	1.7	Fe_5C_2 (I)
	0.17	0.03	183	11.2	Fe_5C_2 (II)
SrFeSi	0.30	0.02	485	24.3	Fe_3O_4 (A)
	0.68	0.01	457	44.0	Fe_3O_4 (B)
	0.20	0.01	213	7.5	Fe_5C_2 (I)
	0.20	0.01	175	4.5	Fe_5C_2 (II)
	0.30	0.02	110	2.4	Fe_5C_2 (III)
	0.70	0.85		17.3	Fe^{2+}
KFeSi	0.33	0.05	486	24.5	Fe_3O_4 (A)
	0.70	0.02	456	44.8	Fe_3O_4 (B)
	0.32	0.01	221	6.7	Fe_5C_2 (I)
	0.19	0.12	182	16.7	Fe_5C_2 (II)
	0.35	0.00	110	7.3	Fe_5C_2 (III)

[a]Max error = ±1 %

of catalysts in syngas, while the promotion of strontium is less effective than that of potassium.

3.4 TPH

The curves of CH_4 evolution during TPH process are depicted in Fig. 8. It can be seen that the curves for FeSi and SrFeSi catalysts are composed of two peaks lied at 200–500 °C, whereas three intense peaks located at 200–800 °C are observed over KFeSi catalyst. It is evident that the CH_4 formation over KFeSi and SrFeSi catalysts shifts to higher temperature compared to that on the FeSi catalyst. To quantitatively analyze the TPH results, the TPH profiles were fitted with Gaussian fitting and the fitte results are tabulated in Table 5. The peaks at 200–450 °C correspond to the atomic (C_α) and polymeric (C_β) carbonaceous species [33]. The peaks located at 500–600 °C are attributed to iron carbides (C_γ), and peaks lied at above 600 °C are assigned to the graphitic species (C_δ) [34]. As listed in Table 5, it is clearly that only C_α and C_β form on the FeSi catalyst surface. Promotion with strontium leads to the formation of iron carbides species over the catalyst surface. As potassium is introduced into the catalyst, the C_β, C_γ and C_δ species are predominantly generated on the catalyst surface, whereas the C_α almost disappear. These results further confirm that the promotion of potassium and strontium enhances the carburization of catalysts. Furthermore, the shift of CH_4 formation peak to higher temperatures implies that the promotion of potassium and strontium strengthens the surface Fe–C interaction on pre-carburized catalysts and suppresses the hydrogenation of surface carbon

species. However, it should be noted that strontium also exhibits a weaker effect compared to potassium.

3.5 FTS Performance

FTS performance of the catalysts was evaluated under reaction conditions of 260 °C, 1.5 MPa, 2000 h^{-1}, and H_2/CO = 2:1. The influence of strontium and potassium promoters on the FTS activity is presented in Fig. 9. The activity of SrFeSi and FeSi catalysts is nearly identical. Their activity increases slightly and then levels off. The KFeSi catalyst with the highest initial activity increases rapidly to a maximum and then approaches steady state. It is evident that the addition of potassium largely improve the catalyst activity, however, strontium shows no apparent impact on the catalyst activity. The iron carbides are general considered as the main active phases for the FTS reaction [35–38]. Hence, the amount of iron carbides detected with MES could be used to determine the content of FTS active sites to a certain degree. The MES results of reduction catalysts shows that the strontium promoted catalyst has slightly higher content of iron carbides, while the potassium promoted catalyst contains much more content of iron carbides than the FeSi catalyst. In fact, the carburization extent of strontium promoted and unprompted catalysts can be considered at the same level, since only one point five percent of iron carbides is increased by the promotion of strontium. Therefore, the carburization degree of activated catalysts correlates well with the initial activity for the catalysts investigated in present study; the higher carburization extent of the activation catalyst, the higher initial activity. The MES results of used catalysts suggest that after FTS reaction for 145 h, the content of iron carbides for strontium promoted and unprompted catalysts decreases obviously, whereas the level of Fe_3O_4 increases compared to the reduced catalysts, respectively. The oxidation of FeC_x to Fe_3O_4 usually leads to a deactivation of iron-based catalysts [39]. However, the deactivation behavior isn't observed over strontium promoted and unprompted catalysts. Li et al. [35] found that the FTS activity is only affected by the amount of the active sites over the surface of the activated catalysts and unrelated with the carburization degree of catalyst bulk. Niemantsverdriet et al. [40] believed that the carburization of the catalyst bulk does not affect the FTS activity. Therefore, it may be that the oxidation of bulk FeC_x to Fe_3O_4 have no apparent effects on the content of active sites on the strontium promoted and unprompted catalyst surface, leading to an unchanged activity of catalysts during FTS reaction. For the potassium promoted catalyst, the content of iron carbides after reaction for 145 h does not decrease, and increase largely as compared with the reduced catalysts. The increase of iron carbides after reaction would result in improving the amount
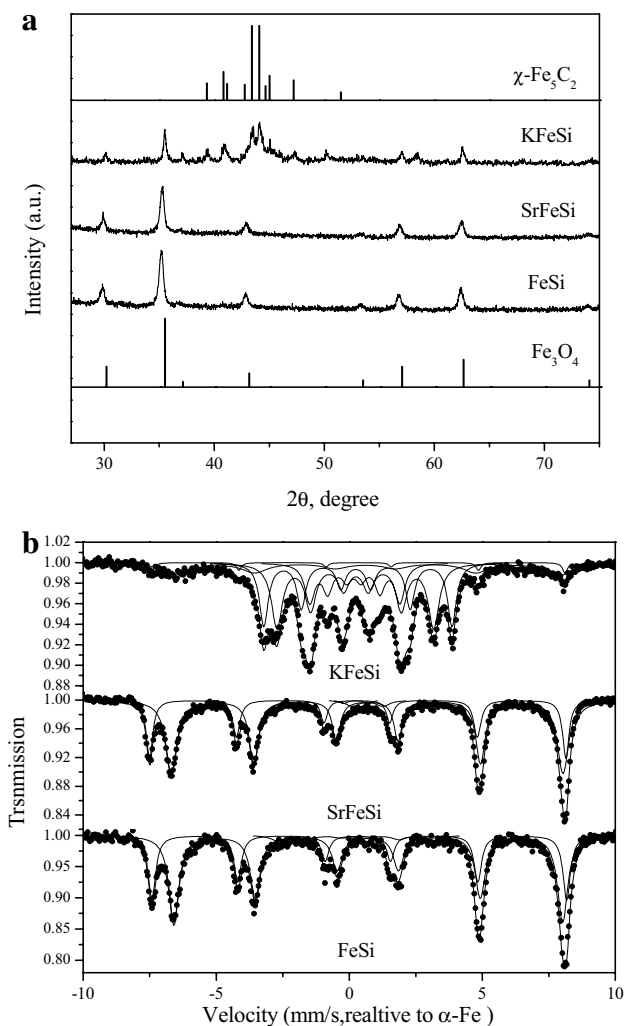
Fig. 5 XRD patterns (**a**) and Mössbauer spectra (**b**) of catalysts after FTS reaction

Fig. 6 H$_2$-TPR (**a**) and CO-TPR (**b**) curves of the catalysts
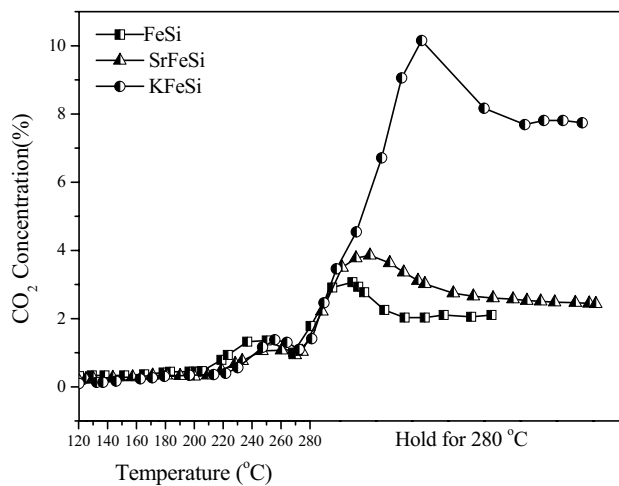
Fig. 7 The CO$_2$ concentration of the catalysts during in situ reduction

Table 4 Mössbauer spectra parameters of catalysts after reaction

Catalysts	IS (mm/s)	QS (mm/s)	Hhf (kOe)	Area[a] (%)	Assignment
FeSi	0.35	0.06	485	33.4	Fe$_3$O$_4$ (A)
	0.71	0.02	454	61.6	Fe$_3$O$_4$ (B)
	0.21	0.12	184	5.0	Fe$_5$C$_2$ (II)
SrFeSi	0.30	0.03	487	29.7	Fe$_3$O$_4$ (A)
	0.67	0.00	458	66.3	Fe$_3$O$_4$ (B)
	0.25	0.94		1.0	Fe^{3+}
	0.69	1.16		3.0	Fe^{2+}
KFeSi	0.37	0.06	480	6.9	Fe$_3$O$_4$ (A)
	0.65	0.00	455	3.8	Fe$_3$O$_4$ (B)
	0.29	0.08	220	32.8	Fe$_5$C$_2$ (I)
	0.23	0.05	189	22.4	Fe$_5$C$_2$ (II)
	0.21	0.06	106	21.0	Fe$_5$C$_2$ (III)
	0.23	0.05	175	13.2	Fe$_{2.2}$C

[a]Max error = ±1

of active sites over potassium promoted catalyst surface, which is responsible for the highest activity observed over potassium promoted catalyst.
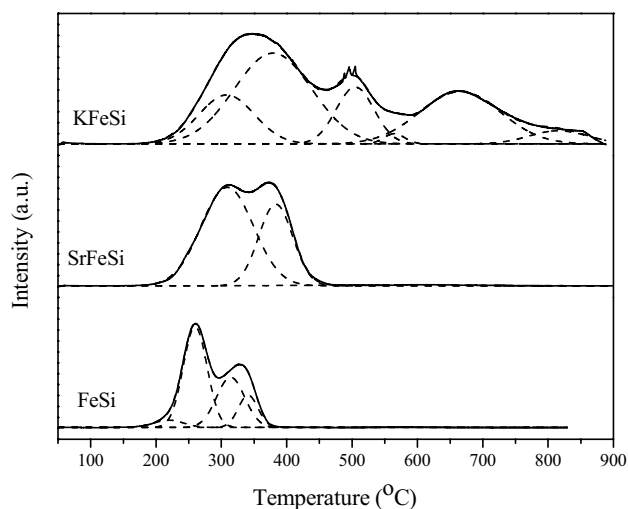
Fig. 8 TPH profiles of the catalysts carburized in 5 % CO/95 % He at 300 °C for 10 h

Table 5 The amounts of carbon species for the carburized catalysts in TPH

Catalysts	Carbon species					
	Atomic and polymeric (C_α and C_β)		Bulk carbides (C_γ)		Graphitic (C_δ)	
FeSi						
Peak (°C)	219	260	314	341		
Area (e^{-7})	9.7	105.4	61.8	27.7		
SrFeSi						
Peak (°C)			309	383	564	
Area (e^{-7})			226.6	121.8	7.13	
KFeSi						
Peak (°C)			308	379	505 565	665 816
Area (e^{-7})			118.1	308.3	94.7 9.4	185.7 33.4

The amounts of carbon species were measured from the area under the corresponding peak

A reversible WGS reaction accompanies the FTS reaction over iron catalyst. Because iron catalyst is active for WGS reaction, which can consume excessive CO and produce hydrogen during FTS, iron catalyst can be directly used to convert syngas with a low H_2/CO ratio, as that produced by coal gasification. The Q_{WGS} value and CO_2 selectivity are normally used to monitor the activity of WGS. As shown in Fig. 10, the promotion of potassium results in the highest Q_{WGS} value and CO_2 selectivity on the catalyst, whereas strontium is less promotional on the WGS activity. WGS reaction could consume a part of water generated during FTS reaction, leading to the low pressure of water vapor in the reactor. Meanwhile, water generated during FTS reaction is reported to be the origin of the oxidation of iron carbides. Satterfield et al. [39] found that the addition
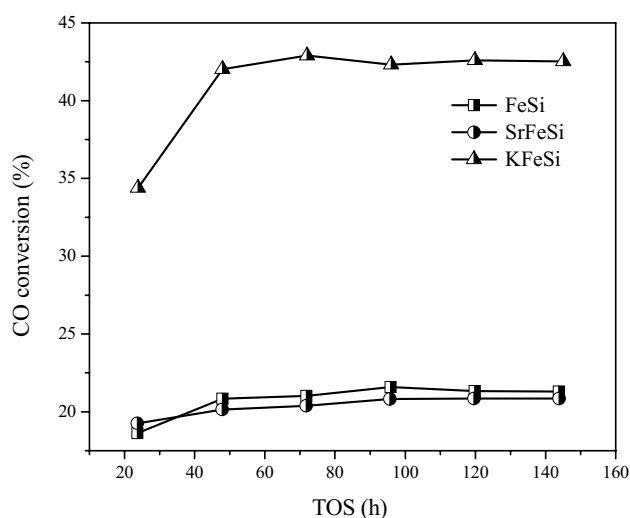

Fig. 9 CO conversion of catalysts

of water on the iron-based catalysts for FTS in slurry reactor would facilitate the oxidation of iron carbides to Fe_3O_4 and result in a decrease of iron carbides and metallic iron. Thus, the WGS reaction remarkably affects on the iron phase composition during FTS reaction. The content of iron carbides increases with increasing the WGS activity due to the low pressure of water vapor in the reactor during FTS reaction. Therefore, the high stability of iron carbides in the KFeSi catalyst during FTS reaction could be ascribed to the high WGS activity. In contrast, the low WGS activity of SrFeSi and FeSi catalysts leads to the poor stability of iron carbides.

The methane and heavy hydrocarbons (C_5^+) selectivities of catalysts are presented in Fig. 11. Detailed hydrocarbon distributions at TOS of 72 and 144 h are given in Table 6. Ihe selectivity of methane decline, while the heavy
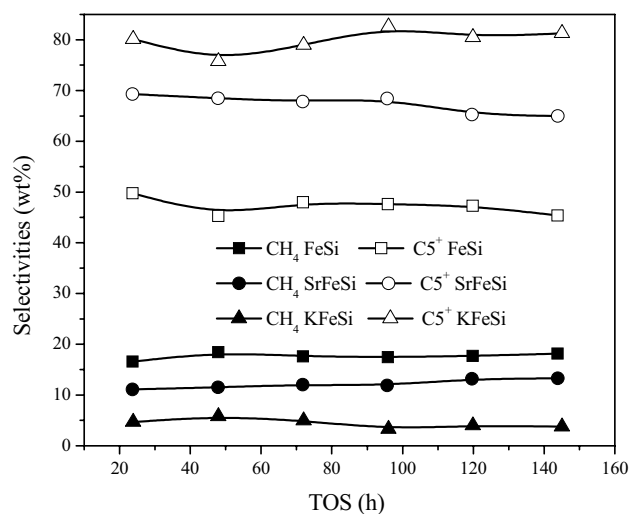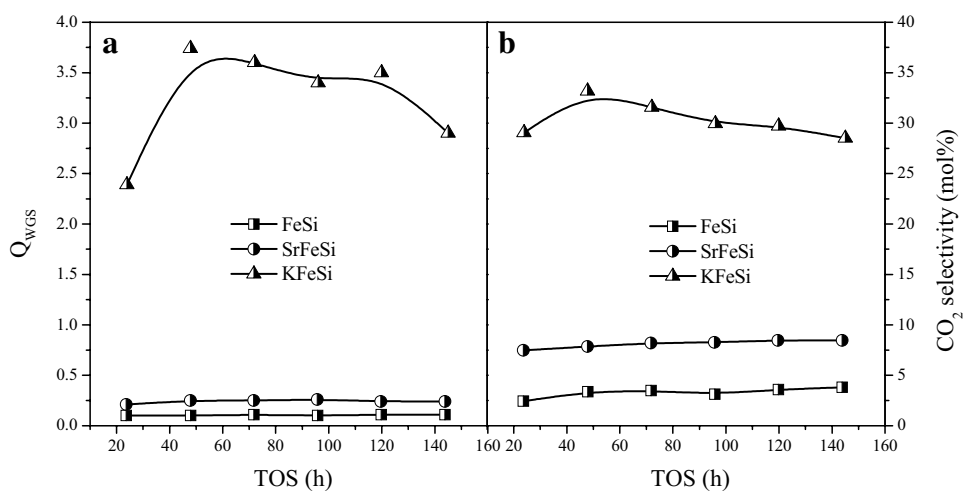

Fig. 11 CH_4 and C_5^+ selectivities of the catalysts

Fig. 10 The variation of **a** Q_{WGS} and **b** CO_2 selectivity with time on stream

Table 6 Activities and hydrocarbon selectivities of catalysts

Catalysts	FeSi		SrFeSi		KFeSi	
TOS (h)	72	144	72	144	72	145
CO conversion (%)	21.01	21.30	20.38	20.84	42.90	42.52
H_2/CO exit ratio	2.12	2.13	1.89	1.90	2.82	2.76
CO_2 selectivity (mol%)	3.48	3.80	8.20	8.46	31.56	28.50
$Kp = P_{CO_2}P_{H_2} / P_{CO} / P_{H_2O}$	0.11	0.11	0.25	0.24	3.60	2.90
HC selectivity (wt%)						
CH_4	17.39	18.06	11.98	13.29	5.01	3.78
C_2–C_4	33.97	36.26	20.15	21.72	16.25	15.12
C_5^+	48.64	45.68	67.87	64.99	78.74	81.10
$C^=_{2-4}/Co_{2-4}$	0.44	0.44	0.57	0.55	0.74	0.75
$C^=_{5-11}/Co_{5-11}$	0.39	0.38	0.42	0.43	0.58	0.64

Reaction conditions: 260 °C, 1.5 MPa, $H_2/CO = 2.0$, GHSV = 2000 h^{-1} and of TOS ca. 145 h

HC hydrocarbon

hydrocarbons (C_5^+) and olefins selectivities increase in turn of FeSi, SrFeSi and KFeSi catalysts. It is obvious that both strontium and potassium improve the formation of long-chain hydrocarbons and olefins, however, strontium is less effective. Surface H/C ratio plays an important role in determining the product distribution of iron-based FTS catalysts [5, 12, 32]. Low surface H/C ratio would enhance the chain propagation reaction and cause an increase in long-chain hydrocarbons selectivity [41]. The addition of strontium and potassium would suppress the H_2 adsorption but facilitates the adsorption of CO, leading to a low surface H/C ratio and weak ability of hydrogenation. In the forgoing sections, the TPH results also demonstrated the fact that the promotion of potassium and strontium strengthens the surface Fe–C interaction and suppresses the hydrogenation of surface carbon species. As a result, high selectivities of heavy weight products and olefin are obtained for strontium and potassium promoted catalysts. The influence of strontium and potassium on the surface H/C ratio is perhaps result from their

basicity or electron donation ability. Potassium is reported to decrease the surface work function of iron and facilitate the dissociation of CO [42–44]. This is due to the quite low ionization potential (4.39 eV) of potassium, which make it easily give out outer shell electron to iron surface [45]. The ionization potential (5.69 eV) of strontium is also lower than that of iron (7.87 eV). Therefore, strontium could also give the outer-shell electrons to iron species in catalysts, leading to an electron rich state of iron species. The electron enrichment of iron species would inhibit H_2 adsorption but enhance the dissociative adsorption of CO, which results in a decreased of H/C ratio on the catalyst surfaces. The decreased surface H/C ratio facilitates the formation of long chain hydrocarbons. However, the ionization potential of strontium is higher than that of potassium, hence, strontium has weaker influences on suppressing H_2 adsorption and facilitating CO dissociative adsorption. Therefore, strontium is less effective on tuning the product distribution than potassium.

4 Conclusion

The ability of strontium as a chemical promoter in the iron-based FTS catalyst was studied. Its promotional effects were compared with those of potassium. It was found that strontium showed similar promotional effects to those of potassium as analysed from the Raman, XRD, MES, H_2/CO-TPR and TPH results. Strontium and potassium strengthened Fe–O bonds of iron oxide species, resulting in inhibitting the removal of oxygen from iron oxide. Both of them facilitated the reduction and carbonization of catalysts in CO and syngas atmosphere, suppressed the hydrogenation of surface carbon species, however, strontium is less effective than potassium. Besides, strontium improved the dispersion of iron oxide. In the FTS reaction, strontium had no significantly influence on the FTS and WGS activity, facilitated the oxidation of iron carbides to Fe_3O_4, while potassium significantly improved the FTS and WGS activity and inhibited the oxidation of iron carbide. Both of strontium and potassium were effective promoters to decrease the selectivities to methane but enhance the formation of olefin and long-chain products, anyway, strontium exhibited a weaker effect compared to potassium.

References

1. Zhang QH, Kang JC, Wang Y (2010) ChemCatChem 2:1030–1058
2. Graf B, Schulte H, Muhler M (2010) J Catal 276:66–75
3. Liu KK, Suo HY, Zhang CH, Xu J, Yang Y, Xiang HW, Li YW (2010) Catal Commun 12:137–141
4. Lohitharn N, Goodwin Jr. JG, Lotero E (2008) J Catal 255:104–113
5. Bukur DB, Mukesh D, Patel SA (1990) Ind Eng Chem Res 29:194–204
6. Huo CF, Li YW, Wang JG, Jiao HJ (2009) J Am Chem Soc 131:14713–14721
7. Lohitharn N, Goodwin Jr. JG (2008) J Catal 260:7–16
8. Raje AP, O'Brien RJ, Davis BH (1998) J Catal 180:36–43
9. Miller DG, Moskovits M (1988) J Phys Chem 92:6081–6085
10. Rankin JL, Bartholomew CH (1986) J Catal 100:533–540
11. Arakawa H, Bell AT (1983) Ind Eng Chem Process Des Dev 22:97–103
12. Yang Y, Xiang HW, Xu YY, Bai L, Li YW (2004) Appl Catal A Gen 266:181–194
13. Zhao GY, Zhang CH, Qin SD, Xiang HW, Li YW (2008) J Mol Catal A Chem 286:137–142
14. Dry ME, Oosthuizen GJ (1968) J Catal 11:18–24
15. Storch HH, Golumbic N, Anderson RB (1951) The Fischer–Tropsch and related synthesis. Wiley, New York
16. Ngantsoue-Hoc W, Zhang YQ, O'Brien RJ, Luo MS, Davis BH (2002) Appl Catal A Gen 236:77–89
17. Lide DR (2003) CRC handbook of chemistry and physics, 84th edn. CRC Press, Boca Raton
18. Cagnoli MV, Marchetti SG, Gallegos NG, Alvarez AM, Mercader RC (1991) Mater Chem Phys 27:403–418
19. Gallegos NG, Alvarez AM, Cagnoli MV, Bengoa JF, Marchetti SG, Mercader RC, Yeramian AA (1996) J Catal 161:132–142
20. Tao ZC, Yang Y, Zhang CH, Li TZ, Wang JH, Wan HJ, Xiang HW, Li YW (2006) Catal Commun 7:1061–1066
21. Yang J, Sun YC, Tang Y, Liu Y, Wang HL, Tian L, Wang H, Zhang ZX, Xiang HW, Li YW (2006) J Mol Catal A Chem 245:26–36
22. Pour AN, Shahri SMK, Bozorgzadeh HR, Zamani Y, Tavasoli A, Marvast MA (2008) Appl Catal A Gen 348:201–208
23. Luo M, Davis BH (2003) Appl Catal A Gen 246:171–181
24. Li JF, Zhang CH, Cheng XF, Qing M, Xu J, Wu BS, Yang Y, Li YW (2013) Appl Catal A Gen 464–465:10–19
25. Zhang CH, Yang Y, Teng BT, Li TZ, Zheng HY, Xiang HW, Li YW (2006) J Catal 237:405–415
26. de Faria DLA, Silva SV, de Oliveira MT (1997) J Raman Spectrosc 28:873–878
27. Yang Y, Xiang HW, Tian L, Wang H, Zhang CH, Tao ZC, Xu YY, Zhong B, Li YW (2005) Appl Catal A Gen 284:105–122
28. Redl FX, Black CT, Papaefthymiou GC, Sandstrom RL, O'Brien SP (2004) J Am Chem Soc 126:14583–14599
29. Suo HY, Wang SG, Zhang CH, Xu J, Wu BS, Yang Y, Xiang HW, Li YW (2012) J Catal 286:111–123
30. Wan HJ, Wu BS, Zhang CH, Xiang HW, Li YW (2008) J Mol Catal A Chem 283:33–42
31. Li SZ, Li AW, Krishnamoorthy S, Iglesia E (2001) Catal Lett 77:197–206
32. Zhang CH, Zhao GY, Liu KK, Yang Y, Xiang HW, Li YW (2010) J Mol Catal A Chem 328:35–43
33. Ahlafi H, Bennett CO, Bianchi D (1992) J Catal 133:83–93
34. Xu J, Bartholomew CH (2005) J Phys Chem B 109:2392–2403
35. Li SZ, Krishnamoorthy S, Li AW, Meitzner GD, Iglesia E (2002) J Catal 206:202–217
36. Li SZ, Meitzner GD, Iglesia E (2001) J Phys Chem B 105:5743–5750
37. Bukur DB, Rosynek MP, Li CP, Wang DJ, Rao KRPM, Huffman GP (1995) J Catal 155:353–365
38. Bukur DB, Lang XS, Ding YJ (1999) Appl Catal A Gen 186:255–275
39. Satterfield CN, Hanlon RT, Tung SE, Zou ZM, Papaefthymiou GC (1986) Ind Eng Chem Prod Res Dev 25:407–411
40. Niemantsverdriet JW, der Kraan AMV, Dijk WLV, Baan HSV (1980) J Phys Chem 84:3363–3370
41. Claeys M, Van Steen E (2004) Stud Surf Sci Catal 152:601–680
42. Benziger J, Madix RJ (1980) Surf Sci 94:119–153
43. Broden G, Gafner G, Bonzel HP (1979) Surf Sci 84:295–314
44. Lee SB, Weiss M, Etl G (1981) Surf Sci 108:357–367
45. Kiskinova MP (1991) Stud Surf Sci Catal 70:169–283